Electrochemical and structural behavior of trirutile-derived FeF$_3$ during sodiation and desodiation

Yayun Zheng,[†] Jinkwang Hwang,[†,‡] Kazuhiko Matsumoto*[,†,‡] and Rika Hagiwara[†,‡]

†Graduate School of Energy Science, Kyoto University, Yoshida-Honmachi, Sakyo-ku, Kyoto 606-8501, Japan

‡ Unit of Elements Strategy Initiative for Catalysts & Batteries (ESICB), Kyoto University, Katsura, Kyoto 615-8510, Japan.

ABSTRACT: Despite the significant advances in the Li−Fe−F systems for lithium-ion batteries, the investigation on the Na−Fe−F systems for sodium-ion batteries is still insufficient. Herein, trirutile-derived FeF_3 prepared through electrochemical delithiation of trirutile $Li_{0.5}FeF_3$ has been examined as the positive electrode of sodium-ion batteries at 90 °C with a thermally stable ionic liquid electrolyte to shed light on the structural evolutions occurring during sodiation-desodiation for the first time. Synchrotron X-ray diffraction revealed that the reversible topotactic extraction/insertion of 0.2 Na^+ proceeds during cycling between 2.6−4.0 V, which triggers a two-phase reaction between tetragonal Na_xFeF_3 and tetragonal FeF_3. A lower cutoff voltage of 2.3−4.0 V induces a partial structural transition from the tetragonal FeF_3 into the cubic FeF_3 along with cycling, where the topotactic Na^+ extraction/insertion not only occurs in the tetragonal structure, but also involve the reversible phase transformation between orthorhombic $NaFeF_3$ and cubic FeF_3 after several cycles.

INTRODUCTION

Metal fluoride compounds have gained eminence as high energy-density electrode materials for secondary batteries owing to the high electronegativity of fluorine compared to the conventional polyanionic, sulfide, and oxide compounds.[1-3] Notably, iron fluorides have garnered interest as positive electrode materials on account of their low costs, high operating voltages and theoretical capacities.[4-8] In particular, the high operating voltages implies the metal fluoride and related materials can possibly achieve high energy density compared with other typical positive electrode materials.[9-12] However, their practical application is impeded by low electrochemical kinetics. As such, the exploration of new structural forms of iron fluorides through rational design will be vital to their successful deployment into practical applications.

In the search for reliable battery systems, sodium-ion batteries (SIBs) have also gained traction due to their high performance and the abundance of Na resources.[13-15] At present, the reaction mechanisms of FeF_3 in lithium-ion batteries (LIBs) have been extensively studied through both experimental and theoretical techniques,[16-22] but that in SIBs remain vastly underexplored.[4,6] Table 1 lists noteworthy works on FeF_3 and $NaFeF_3$ positive electrodes in SIBs. Experimental reports on FeF_3 electrodes have demonstrated that the reduction of Fe^{3+} to Fe^{2+} involves a classical insertion process occurring between FeF_3 and $NaFeF_3$. However, no experimental evidence on the phase structures or the existence of a Na_xFeF_3 intermediate phase has been reported to date.[23-24] Nonetheless, other studies

on $NaFeF_3$ have provided insight into the phase evolutions during the desodiation-sodiation processes. For instance, density functional theory calculations on the orthorhombic $NaFeF_3$ (*Pnma*) revealed that the oxidation of Fe^{2+} to Fe^{3+} was engendered by Na^+ extraction from the orthorhombic $NaFeF_3$ to form fully desodiated FeF_3 (*Pnma*): a slightly more stable phase than the trigonal ($R\bar{3}c$) and cubic ($Pm\bar{3}m$) phases.[25] The theoretical works further envisaged an energetically stable, intermediate phase of orthorhombic $Na_{0.5}FeF_3$, as a line compound in the extraction process.[25-26] A recent experimental work on nano-sized materials reported a phase transformation from orthorhombic $NaFeF_3$ (*Pnma*) to cubic FeF_3 ($Pm\bar{3}m$), albeit without forming trirutile $Na_{0.5}FeF_3$.[27-28] Although the phase transformation was not observed, this study was the first to mention trirutile $Na_{0.5}FeF_3$ in the context of the Na-Fe-F system.

In contrast, trirutile $Li_{0.5}FeF_3$ (space group: $P4_2/mnm$) is a well-studied intermediate phase in the lithiation process of FeF_3 ($R\bar{3}c$), even though it has not been clearly observed by X-ray diffraction (XRD).[18,20] A recent study on the reaction mechanisms of the trirutile $Li_{0.5}FeF_3$ as a positive electrode for LIBs operating at 90 °C found the initial delithiation of the trirutile $Li_{0.5}FeF_3$ results in a tetragonal phase (also known as trirutile-derived FeF_3, and hereafter, tetragonal-1 FeF_3).[29] Further, at a certain cutoff voltage, reversible charge-discharge cycles between the trirutile $Li_{0.5}FeF_3$ and tetragonal-1 FeF_3 were noted to occur via a two-phase topotactic reaction.

Given that the tetragonal-1 FeF_3 phase has not been exploited as a positive electrode in SIBs, the findings from the Li system emphasize the importance of understanding tetragonal-1 FeF_3 phase evolutions as the means to decipher the iron fluoride mechanisms in the Na-Fe-F system for future material designs. More importantly, the reports predict the possibility of observing the reversible Na^+ extraction/insertion from/into the tritutile-type structure with the tetragonal-1 FeF_3 phase as the starting material. Therefore, in an attempt to explicate the phase evolutions occurring in the Na-Fe-F system, we investigate the electrochemical properties and the reaction mechanisms of the tetragonal-1 FeF_3 in the Na system through charge-discharge tests, galvanostatic intermittent titration (GITT) tests, and synchrotron XRD techniques.

EXPERIMENTAL SECTION

All reagents used in this work were stored and handled in a glove box filled with dry and deoxygenated Ar (oxygen and water level < 1 ppm). Tetrahydrofuran (THF; dehydrated, Wako Pure Chemical Industries, water content < 10 ppm, stabilizer-free), Li metal (Sigma-Aldrich, purity 99.95%), and Na metal (Sigma-Aldrich, purity 99.95%) were used as purchased. Acetylene black (AB; Wako Pure Chemical Industries, purity > 99.99%) and poly(tetrafluoroethylene) (PTFE; Sigma-Aldrich, Inc.; particle size: ca. 200 μm) were dried under vacuum at 120 °C before storing in the glove box. The FSA salts, Li[FSA]

(FSA⁻: bis(fluorosulfonyl)amide, Kishida Chemical, purity > 99%) and Na[FSA] (Mitsubishi Materials Electronic Chemicals, purity > 99%) as well as [C_2C_1im][FSA] (C_2C_1im⁺: 1-ethyl-3-methylimidazolium, Kanto Chemical, purity > 99.9%) were dried under vacuum at 80 °C. Battery-grade 1 M $NaPF_6$/EC:DMC (1:1 in volume, Kishida Chemical Co. Ltd.; EC: ethylene carbonate; DMC: dimethyl carbonate) organic electrolyte was used as purchased.

Trirutile $Li_{0.5}FeF_3$ was prepared by the ball-milling method according to the procedure described in previous work.[29] Tetragonal-1 FeF_3 was prepared by the electrochemical delithiation of the trirutile $Li_{0.5}FeF_3$ electrode (Figure 1). The electrode was fabricated by pressing a mixture of 95 wt% ball-milled composite $Li_{0.5}FeF_3$/AB (75:25 wt%) and 5 wt% PTFE onto an Al mesh (13 mm in diameter). The electrochemical delithiation of trirutile $Li_{0.5}FeF_3$ to tetragonal-1 FeF_3 was carried out at a current density of 10 mA g⁻¹ in a 2032-type half-cell with a Li metal counter electrode fixed on stainless steel (SS316L) plate current collector. The Li[FSA]-[C_2C_1im][FSA] ionic liquid (IL) in a molar ratio of 30:70 was used as the electrolyte. After electrochemical delithiation, the cell was disassembled in the glove box. The obtained FeF_3 electrode was then washed with THF and dried under vacuum at room temperature for 12 h. Sodiation-desodiation properties were analyzed in a 2032-type half-cell using the tetragonal-1 FeF_3 positive electrode, a Na metal fixed on Al plate current collector as the counter electrode, and the Na[FSA]-[C_2C_1im][FSA] IL in a molar ratio of 30:70 as the electrolyte. The glass microfiber separator (Whatman,

GF/A; 16 mm in diameter and 260 μm in thickness) was immersed in the IL electrolyte under vacuum at 90 °C for 12 h prior to the cell assembling. For all the cells, the applied current and the resulting capacity were calculated based on the weight of the pristine $Li_{0.5}FeF_3$ electrode (2.00 mg cm^{-2}) according to the following equation:

Capacity (mAh g^{-1}) = Current (mA) x Time (h) / Mass of the active material (g)

All electrochemical measurements were performed at an elevated temperature of 90 °C with the aid of the thermally stable IL electrolyte. The Na cell was galvanostatically cycled at 21.4 mA g^{-1} in two voltage ranges of 2.6–4.0 and 2.3–4.0 V. A GITT determined the overpotentials by repeatedly monitoring the voltage relaxation in the open-circuit state immediately after charging or discharging to a certain state. The cell for GITT was charged or discharged at 10 mA g^{-1} for 1 h followed by 5-hour open circuit relaxation between 2.3−4.0 V. Cyclic voltammetry was performed using a VSP potentiostat (Bio-Logic) at a scan rate of 0.1 mV s^{-1} at 90 °C, in which the half-cell was firstly scanned from open circuit voltage to lower voltage in both two voltage ranges.

The Li and Fe contents in the tetragonal-1 FeF_3 were determined after dissolution with sulfuric, nitric, and perchloric acids by atomic absorption spectrometry (AAS, Hitachi Z-2300) and inductively coupled plasma−atomic emission spectroscopy (ICP−AES, Hitachi

PS3520VDD II), respectively. The crystalline phases of the charged and discharged electrodes were analyzed by XRD at the BL5S2 beam line of Aichi Synchrotron Radiation Center (wavelength of 0.88589 Å) equipped with a PILATUS 100K two-dimensional detector. The charged and discharged electrode samples were washed with THF, vacuum-dried at room temperature, and then sealed in Lindeman glass capillaries for synchrotron XRD measurements. Structural parameters were refined with the Rietveld refinement by curve-fitting using the GSAS data analysis software.[30] The crystal structure was visualized by the VESTA program.[31]

RESULTS AND DISCUSSION

The tetragonal-1 FeF_3 phase was electrochemically prepared by delithiating trirutile $Li_{0.5}FeF_3$ with the aid of a thermally stable IL electrolyte, $Li[FSA]$-$[C_2C_1im][FSA]$ (30:70 in mol), at a current density of 10 mA g^{-1} (Figure 1).[32] The process was conducted at 90 °C in light of previous study that established high temperature to be essential in activating the delithiation reaction.[29] As displayed in Figure 1, the delithiation occurred via a two-phase process marked by a plateau at 4.0 V. Synchrotron XRD analysis performed at the end of the delithiation confirmed the formation of a tetragonal-1 FeF_3 phase containing trirutile $Li_{0.5}FeF_3$, rutile FeF_2 and trigonal FeF_3 ($R\bar{3}c$) impurities. The

nominal composition of Li_xFeF_3 is calculated to be $x = 0.11$ according to the capacity,[29] and 0.14 based on the AAS and ICP−AES.

The tetragonal-1 FeF_3 electrode was washed, dried, and transferred into a Na half-cell comprising a Na metal counter electrode and the $Na[FSA]$-$[C_2C_1im][FSA]$ (30:70 in mol) IL electrolyte. The IL was selected for its ability to derive stable charge-discharge behavior from various electrode materials at elevated temperatures.[33-35] Electrochemical properties of the tetragonal-1 FeF_3 were investigated at room temperature in IL and organic electrolytes (Figure S1 in the Supporting Information (SI)). At room temperature (25 °C), tetragonal-1 FeF_3 exhibits poor electrochemical activity in both electrolytes in Na system (Figure S1, SI). The similar shape of charge-discharge curves is observed during 20 cycles with continuous capacity fading. The reason for the poor capacity is considered to be the slow phase transition limited by the large particle size of pristine trirutile $Li_{0.5}FeF_3$ material.[29] All these observations suggest that the elevated temperature is essential in order to bring out the electrochemical activity of tetragonal-1 FeF_3 in the Na system, in line with the report on the Li system.[29,33-35] Thus, the charge-discharge behavior of the tetragonal-1 FeF_3 was examined in IL electrolyte at 90 °C (Figures 2 and 3). The electrode was pre-discharged to 2.6 V (Figure S2, SI) and thereafter investigated in the 2.6–4.0 V (Figure 2a and b). The initial charge-discharge cycle attains a discharge capacity of 53.2 mAh g^{-1} and is marked by a pair of plateaus (3.8/3.6 V, see dQ/dV plot in Figure 2b). The plateaus correspond to a two-phase reaction between sodiated

tetragonal Na_xFeF_3 phase and desodiated tetragonal FeF_3 phase caused by the reversible extraction/insertion of Na^+ from/into the tetragonal structure.[29] The sloping voltage profile at the low voltage means the Na^+ extraction/insertion of Na^+ from/into the tetragonal structure in a single-phase reaction without phase change. Although the capacity is limited, the shape of the charge-discharge curve remains unchanged during 20 cycles. Further cycling produces superposing charge-discharge curves with no changes in shape and a reversible capacity of 47.3 mAh g^{-1} at the 50th cycle (Figures S3 and S4, SI). These results evince the reversible insertion reactions of the tetragonal-1 FeF_3 with 0.2 Na^+ (theoretically 118 mAh g^{-1} for $0.5e^-$ transfer) between 2.6–4.0 V. The cyclic voltammetry (CV) of the Na/tetragonal-1 FeF_3 cell clearly shows the redox peaks at 3.90/3.51 V for 10 cycles (Figure 2c), which is consistent with the preservation of charge-discharge curves and dQ/dV plots in the same cut-off voltage during cycling (Figure 2a and b).

The tetragonal-1 FeF_3 was further examined in the extended cutoff range of 2.3−4.0 V (Figure 3). A full plateau, which appears around 2.57 V during the pre-discharge to 2.3 V (Figure S5, SI), is noted to disappear in the subsequent sodiation processes (Figure 3a). This one-time plateau corresponds to the conversion reaction of the residual trirutile $Li_{0.5}FeF_3$ into rutile FeF_2 and alkali metal fluorides (LiF and NaF).[29] As observed from the resembling charge-discharge curves to the one in the 2.6–4.0 V range, an analogous desodiation-sodiation behavior related to the reversible extraction/insertion of Na^+ in the

tetragonal structure is confirmed to occur during the first two cycles in the 2.3–4.0 V range. The appearance of a short plateau from 2.5 to 2.7 V during the charge process is considered to be the reconversion reaction from rutile FeF_2 and LiF (NaF) to tetragonal Li_xFeF_3 with disordered trirutile structure. The trirutile $Li_{0.5}FeF_3$ work has proved that the conversion reaction shows poor reversibility,[29] and the amount of rutile FeF_2 and LiF (NaF) involved in the reconversion reaction in Na system is very limited as indicated by the weak redox peaks for the subsequent few cycles (see dQ/dV plot in Figure 3b and CV in Figure 3c). After several cycling, two pairs of new plateaus (3.41/3.16 V and 3.05/2.94 V) are observed to emerge around 10th cycle (see charge-discharge curves and the dQ/dV curves in Figure 3a,b and Figure S6a,b, SI). These new plateaus are also observed thereafter throughout the initial 50 cycles, along with a slight capacity fade (Figures S7 and S8, SI). The CV also shows the new redox peaks after 5th cycle (Figure 3c), as suggested by the changes on the charge-discharge curves and dQ/dV plots in the same cut-off voltage during cycling (Figure 3a and b). All these observations demonstrate a gradual transition in the reaction mechanisms with continued cycling. Significant progresses in the electrochemical properties were made on FeF_3 positive electrode materials for sodium-ion batteries,[4,6,24] but the mechanism behind the electrochemical insertion of Na into FeF_3 is still poorly covered in the previous literature. The stable cycle performances of the tetragonal-1 FeF_3 between 2.3–4.0 V and 2.6–4.0 V over 50 cycles

suggest that this electrode material is suitable for clarifying the reaction mechanism of tetragonal structure during sodiation-desodiation processes.

Figure 4 shows the GITT profiles of the Na/tetragonal-1 FeF_3 cell during the pre-discharge, 1st, and 10th charge-discharge cycles. The voltage after each relaxation process shows a short plateau around 2.6 V during the pre-discharge (Figure 4a), which is due to the conversion reaction of the residual trirutile $Li_{0.5}FeF_3$ to rutile FeF_2 and LiF as mentioned above. The voltage after relaxation during the first charge gradually increases with increasing the state of charge (SOC) and exhibits a plateau at 3.7 V. Considering the GITT profile of the trirutile $Li_{0.5}FeF_3$,[29] this flat plateau around 3.7 V is assigned to the two-phase reaction between Na-rich and Na-deficient tetragonal phases caused by desodiation in the tetragonal structure. The first discharge profile is free from the short plateau at 2.6 V observed in the pre-discharge. The GITT curve at the 10th cycle (Figure 4b) shows different profiles from the first cycle with smaller voltage hysteresis, which evidences the change of the reaction mechanism during cycling.

For further insight into the reaction mechanisms, synchrotron XRD measurements were performed on the tetragonal-1 FeF_3 electrodes at different states of charge (SOCs) between 2.3−4.0 V (Figure 5). The corresponding voltage-time profile is shown in Figure 5a. XRD patterns A and B denote the pristine trirutile $Li_{0.5}FeF_3$ and the tetragonal-1 FeF_3 electrode, respectively (Figure 5b). In the previous work on the Li system,[29] the tetragonal-1 FeF_3 and the trirutile $Li_{0.5}FeF_3$ were reported to have similar crystal

structures except that the tetragonal-1 FeF_3 had a vacant $2a$ site, larger a- and b-parameters, and a smaller c-parameter than the trirutile $Li_{0.5}FeF_3$ (trirutile $Li_{0.5}FeF_3$: a = 4.6798(1) Å, c = 9.3095(4) Å and tetragonal-1 FeF_3: a = 4.7718(3) Å, c = 8.8557(1) Å).

In the current study, pre-discharging the tetragonal-1 FeF_3 phase to 2.6 V (Pattern 1) in the Na system results in the disappearance of the tetragonal-1 phase and the appearance of multiple phases with broad diffraction peaks. Rietveld refinement of Pattern 1 (see Figure S9a, SI and Table 2) confirms that the main phase of the resulting material is related to a sodiated tetragonal Na_xFeF_3 phase formed by the topotactic insertion of Na^+ into the $2a$ site of the tetragonal-1 FeF_3 (hereafter denote as the sodiated tetragonal-1 Na_xFeF_3). The corresponding crystallographic data (Table 2) reveal that the sodiated tetragonal-1 Na_xFeF_3 phase has a disordered trirutile structure (where the $2a$ site is occupied by Fe with an occupancy ratio of 0.2235) with larger a- and c-parameters than those of tetragonal-1 FeF_3. One of the other phases observed is attributed to rutile FeF_2, formed by the partial sodiation of the residual trirutile $Li_{0.5}FeF_3$. Alkali fluorides (LiF and NaF) are also noted, but their peaks are too weak and broad to be included in the Rietveld refinement.

The sodiated tetragonal-1 Na_xFeF_3 and the rutile FeF_2 phases are also detected in Pattern 2, demonstrating the occurrence of topotactic Na^+ insertion into the tetragonal-1 FeF_3 and a full conversion reaction from trirutile $Li_{0.5}FeF_3$ to rutile FeF_2 and alkali fluorides during the pre-discharge to 2.3 V (see Figure S9b, SI and Table 2). In Pattern 2,

a new broad peak appearing around 12.9°, is assigned to the 002 diffraction of orthorhombic $NaFeF_3$.[25-26] This orthorhombic $NaFeF_3$ is a product of the insertion of extra Na^+ into the tetragonal-1 FeF_3, which suggests that extending the sodiation of the tetragonal-1 FeF_3 to 2.3 V engenders a structural transformation from the tetragonal structure to the orthorhombic structure. In addition, the impurity trigonal FeF_3 in the starting tetragonal-1 FeF_3 is also believed to contribute to the formation of orthorhombic $NaFeF_3$ at the low voltage,[4,6] although its contribution is limited.

After the initial charging to 4.0 V (Pattern 3), a sharp peak appears around 15.2°, which is related to the formation of a desodiated tetragonal phase at the high voltage. However, the diffraction peaks of this tetragonal phase show slightly shift in position compared to those of the initial tetragonal-1 FeF_3 (Pattern B). This reveals that the tetragonal-1 phase is no longer recovered by the desodiation of the multiple-phase mixture of sodiated tetragonal-1 Na_xFeF_3 phase, rutile FeF_2, alkali metal fluorides (LiF and NaF) and the orthorhombic $NaFeF_3$. Rietveld refinement of Pattern 3 (see Figure S9c, SI and Table 2) verifies that the slightly shifted diffraction peaks can be indexed as a disordered trirutile structure (hereafter, tetragonal-2 FeF_3) wherein the $2a$ site is occupied by Fe with an occupancy ratio of 0.4357. The corresponding crystallographic data (Table 2) further reveal that the initial desodiation engenders a 1.2% decrease in the a- lattice parameter and a 6.7% increase in the c- lattice parameter, yielding a 4.1% larger overall volume than the initial tetragonal-1 FeF_3. In the previous study on the Li system, the tetragonal-2 FeF_3

phase was also found to exist in the charged state after the electrode was discharged to 2.5 V.[29] It is worth noting that Pattern 3 also exhibits a peak corresponding to the 012 diffraction of the trigonal FeF_3 ($R\bar{3}c$). This suggests that part of the rutile FeF_2 and the alkali metal fluorides are involved in the formation of the trigonal FeF_3 phase during the charge process.[29,36]

After the first discharge to 2.3 V (Pattern 4), the diffraction pattern resembles that of the pre-discharged electrode (Pattern 2), except for the diffraction peaks of the orthorhombic $NaFeF_3$ which becomes stronger after one cycle, indicating that the amount of orthorhombic $NaFeF_3$ phase increases during the initial discharge. Notably, the increased orthorhombic $NaFeF_3$ is thought to be derived not only from tetragonal-2 FeF_3, but also from trigonal FeF_3.[4,6] Rietveld refinement of Pattern 4 (see Figure S9d, SI and Table 2) also reveals the presence of a sodiated tetragonal Na_xFeF_3 phase with lattice parameters similar to the tetragonal-1 Na_xFeF_3 phase, confirming that the tetragonal-2 FeF_3 is re-sodiated back to tetragonal-1 Na_xFeF_3.

At the charged state of the 10th cycle (Pattern 5), the 100 diffraction peak belonging to the cubic FeF_3 ($Pm\bar{3}m$) is noted at 13.3°,[27] which confirms that the new reaction previously visualized by the new charge-discharge curves is related to a reversible phase transformation from the orthorhombic $NaFeF_3$ ($Pnma$) phase to the cubic FeF_3 ($Pm\bar{3}m$) phase. This is consistent with the previous study on the charge-discharge behavior of the nano-sized orthorhombic $NaFeF_3$.[27-28] Pattern 5 also highlights the presence of a

tetragonal phase (hereafter, tetragonal-3 FeF_3) which exhibits a disordered trirutile structure akin to the tetragonal-2 FeF_3, despite their different lattice parameters due to different Fe occupancies (see Figure S9e, SI and Table 2).

At the discharged state of the 10th cycle (Pattern 6), diffraction peaks related to the sodiated tetragonal Na_xFeF_3, orthorhombic $NaFeF_3$ and rutile FeF_2 are observed. The crystal structure of the sodiated tetragonal Na_xFeF_3 phase is analogous to that of the sodiated tetragonal-1 Na_xFeF_3 but with different lattice parameters (see Figure S9f, SI and Table 2). The formation of the sodiated tetragonal Na_xFeF_3 phase, hereafter denoted as sodiated tetragonal-3 Na_xFeF_3, evinces that the topotactic insertion/extraction of Na^+ into/from the tetragonal phase continues to occur during the sodiation-desodiation processes after 10 cycles. It is worth noting that the presence of the rutile FeF_2 throughout the charge-discharge cycles denotes its partially inactive electrochemical nature, consistent with the observations made in the previous work on trirutile $Li_{0.5}FeF_3$.[29]

Figure 6 summarizes the charge-discharge mechanisms of the tetragonal-1 FeF_3 in the Na system and the changes occurring during cycling in the 2.3−4.0 V range (see Schemes S1 and S2 for the corresponding equations of the redox reaction, SI). First two cycles yield a pair of plateaus around 3.7 V, engendered by a sodiation-desodiation process which mainly involves the topotactic Na^+ insertion/extraction reaction into/from tetragonal-type FeF_3. A conversion reaction from the trirutile $Li_{0.5}FeF_3$ to rutile FeF_2 with alkali metal fluorides and transformation to the orthorhombic $NaFeF_3$ also occur during

16

sodiation, whereas rutile FeF_2 is partially converted to trigonal FeF_3 during the successive desodiation. The two initial cycles only produce small amounts of orthorhombic $NaFeF_3$. However, its quantity formed at 2.3 V progressively increase with continued cycling due to the poor reversibility of the orthorhombic to tetragonal phase transformation. After 10 cycles, the sodiation-desodiation process partially changes to reversible Na^+ insertion and extraction between cubic FeF_3 and orthorhombic $NaFeF_3$ phases—a transition marked by the emergence of new charge-discharge curves, while along with the reversible insertion/extraction reaction into/from the tetragonal phase. It is worth noting that a disordered trirutile structure derived from the starting trirutile structure is discerned at different charged states of the electrode.[29] The remained Li in tetragonal-1 FeF_3 stabilizes the tetragonal structure by avoiding excessive extraction in the trirutile $Li_{0.5}FeF_3$ and is involved in the pre-discharge, first charge forming trigonal FeF_3, and several cycles for the conversion reaction during sodiation-desodiation. After around 10 cycles, the disappearance of the weak redox peaks suggests the remained Li which exists in the form of LiF is inactive in the subsequent charge-discharge processes (dQ/dV plot in Figure 3b and CV in Figure 3c). Significantly, it is demonstrated that the tetragonal-1 FeF_3 theoretically undergoes 0.5 Li^+ insertion to recover trirutile $Li_{0.5}FeF_3$ and further reacts with 0.5 Li^+ to occur a conversion reaction in the Li system between 2.5–4.3 V.[29] Different from the Li system, the tetragonal-1 FeF_3 undergoes Na^+ insertion reaction to form tetragonal Na_xFeF_3 ($x \sim 0.2$) and orthorhombic $NaFeF_3$ at a discharged state similar

to the Li system (2.3 V), instead of the conversion reaction to NaF and FeF_2. The comparison of the tetragonal structure in Li and Na systems demonstrates that the electrochemical responses of the tetragonal structure in Na system are different from that in the Li system. In addition, the electrochemical properties of tetragonal-1 FeF_3 over an extended voltage range of 1.5–4.0 V were investigated (Figures S10 and S11, SI). Extending the low voltage to 1.5 V triggers the conversion reaction to metallic Fe and NaF with a discharge capacity of 404.0 mAh g^{-1}, as indicated by the long plateau around 1.9 V. Cycling between 1.5−4.0 V engenders the capacity fading from 359.2 mAh g^{-1} at the 1st cycle to 160.4 mAh g^{-1} at the 15th cycle, and the appearance of charge-discharge curves resemble those in the 2.3–4.0 V range. These observations indicate that the reaction mechanism in the extended voltage range of 1.5–4.0 V also shows a transition to the reversible phase transformation between orthorhombic $NaFeF_3$ to cubic FeF_3, as observed in the cutoff range of 2.3−4.0 V.

CONCLUSIONS

In summary, we report for the first time a trirutile-derived FeF_3 phase as a positive electrode for SIBs. The formation of disordered trirutile Na_xFeF_3 is confirmed by the presence of a sodiated tetragonal Na_xFeF_3 in the discharged state of the electrode. We also shed light on the reaction mechanisms of the Na-Fe-F system by elucidating the

structural transition between the tetragonal-1 FeF_3 and the cubic FeF_3 phases in the charged states of the electrode during cycling. However, the sodiation-desodiation processes are mired in unexpected reactions caused by impurity phases formed during the preparation of the starting material. Therefore, we postulate that future investigations using a pure-phased sodium iron fluoride composite with the tetragonal structure would provide a better perspective of the Na-Fe-F system.

Table 1. Summary of selected works on FeF_3 and $NaFeF_3$ positive electrodes for sodium-ion batteries.

Year	Existent form	Preparation method	Initial discharge capacity	Crystallographic and electrochemical properties
2009[4]	Trigonal FeF_3 (S.G. $R\bar{3}c$)	Commercial reagent	145 mAh g^{-1} at 1.5 V (A rate of 0.2 mA cm^{-2})	Reversible Fe^{3+}/Fe^{2+} redox reaction
2011[37]	Orthorhombic $NaFeF_3$ (S.G. $Pnma$)	Liquid-phase synthesis	153 mAh g^{-1} between 1.5−4.5 V (19.7 mA g^{-1})	None
2012[38]	Orthorhombic $NaFeF_3$ (S.G. $Pnma$)	Solid-state method	126 mAh g^{-1} between 1.5−4.0 V (A rate of 0.076 mA cm^{-2})	The extraction/insertion of sodium by the reversible lattice vibration
2013[39]	Orthorhombic $NaFeF_3$ (S.G. $Pnma$)	Solid-state method	225 mAh g^{-1} between 1.5−4.5 V (7.5 mA g^{-1})	$NaFeF_3 \rightarrow$ Charged state FeF_3 + Na^+ + e^- (Reversible Na^+ reinsertion)
2013[40]	Orthorhombic $FeF_3 \cdot 0.33H_2O$ (S.G. $Cmcm$)	Solid-solid breakdown method	130 mAh g^{-1} at 1.2 V (23.7 mA g^{-1})	None
2014[23]	In situ generated FeF_3 from FeF_2–RGO	Electrochemical activation	150 mAh g^{-1} at 1.5 V (50 mA g^{-1})	$FeF_3 + Na^+ + e^- \rightleftarrows NaFeF_3$
2014[25]	Orthorhombic $NaFeF_3$ (S.G. $Pnma$)	First-principle density functional theory calculations	None	Orthorhombic $NaFeF_3 \rightarrow$ Orthorhombic $Na_{0.5}FeF_3$ + 0.5 Na^+ + 0.5 $e^- \rightarrow$ Orthorhombic FeF_3 + 0.5 Na^+ + 0.5 e^-
2017[6]	Trigonal FeF_3 (S.G. $R\bar{3}c$)	Single-source molecular precursors	160 mAh g^{-1} at 1.6 V (200 mA g^{-1})	Assume a similar mechanism with the work[23]
2017[26]	Orthorhombic $NaFeF_3$ (S.G. $Pnma$)	Ball milling; density functional calculation	169 mAh g^{-1} at 2 V (A rate of 0.1 mA cm^{-2})	$FeF_3 + 0.5\,Na^+ + 0.5\,e^- \rightarrow Na_{0.5}FeF_3 + 0.5\,Na^+ + 0.5\,e^- \rightarrow NaFeF_3$
2018[24]	Orthorhombic $FeF_3 \cdot 0.33H_2O@$ 3D-OMCs (S.G. $Cmcm$)	Hydrothermal method	386 mAh g^{-1} at 1 V (20 mA g^{-1})	$FeF_3 + Na^+ + e^- \rightarrow NaFeF_3$ (4−1.2 V); $NaFeF_3 + 2\,Na^+ + 2\,e^- \rightarrow 3$ NaF + Fe (1.2−1.0 V)
2018[27]	Orthorhombic $NaFeF_3$ (S.G. $Pnma$)	Microwave-assisted solution synthesis	150 mAh g^{-1} between 2.0−4.0 V (19.7 mA g^{-1})	$NaFeF_3 \rightleftarrows$ Cubic FeF_3 (S.G. $Pm\bar{3}m$) + Na^+ + e^- (Insertion/deinsertion mechanism)

Table 2. Crystallographic parameters of the tetragonal phases for Pattern 1, Pattern 2, Pattern 3, Pattern 4, Pattern 5 and Pattern 6 in Figure 5 obtained by Rietveld refinement.

Refinement results for the sodiated tetragonal-1 Na$_x$FeF$_3$ phase in Pattern 1[a] (S.G. $P4_2/mnm$)						
R_p = 2.93%, R_{wp} = 3.87%						
a = 4.8267(6) Å		c = 9.572(2) Å			V = 223.00(6) Å^3	
Atom	Wyckoff symbol	x	y	z	B_{iso} / Å^2	Occup.
Na	2a	0	0	0	0.5	0.6016
Fe	2a	0	0	0	0.5	0.2235
Fe	4e	0	0	0.3184(7)	0.5	0.8883
F1	4f	0.327(1)	0.327(1)	0	0.5	1
F2	8j	0.2728(9)	0.2728(9)	0.3585(8)	0.5	1

Refinement results for the sodiated tetragonal-1 Na$_x$FeF$_3$ phase in Pattern 2[b] (S.G. $P4_2/mnm$)						
R_p = 3.12%, R_{wp} = 3.94%						
a = 4.846(1) Å		c = 9.596(5) Å			V = 225.4(1) Å^3	
Atom	Wyckoff symbol	x	y	z	B_{iso} / Å^2	Occup.
Na	2a	0	0	0	0.5	0.6493
Fe	2a	0	0	0	0.5	0.2815
Fe	4e	0	0	0.316(2)	0.5	0.8592
F1	4f	0.316(4)	0.316(4)	0	0.5	1
F2	8j	0.247(3)	0.247(3)	0.366(2)	0.5	1

Refinement results for the tetragonal-2 FeF$_3$ phase in Pattern 3[c] (S.G. $P4_2/mnm$)						
R_p = 4.46%, R_{wp} = 5.99%						
a = 4.713(1) Å		c = 9.450(2) Å			V = 209.87(9) Å^3	
Atom	Wyckoff symbol	x	y	z	B_{iso} / Å^2	Occup.
Fe	2a	0	0	0	0.5	0.4357
Fe	4e	0	0	0.3176(7)	0.5	0.7822
F1	4f	0.324(1)	0.324(1)	0	0.5	1
F2	8j	0.2796(9)	0.2796(9)	0.3652(6)	0.5	1

Refinement results for the sodiated tetragonal-1 Na$_x$FeF$_3$ phase in Pattern 4[d] (S.G. $P4_2/mnm$)						
R_p = 3.45%, R_{wp} = 4.28%						
a = 4.843(1) Å		c = 9.600(6) Å			V = 225.1(1) Å^3	
Atom	Wyckoff symbol	x	y	z	B_{iso} / Å^2	Occup.
Na	2a	0	0	0	0.5	0.6535
Fe	2a	0	0	0	0.5	0.3011

Atom	Wyckoff symbol	x	y	z	B_{iso} / Å²	Occup.
Fe	4e	0	0	0.345(2)	0.5	0.8495
F1	4f	0.301(5)	0.301(5)	0	0.5	1
F2	8j	0.261(4)	0.261(4)	0.297(2)	0.5	1

Refinement results for the tetragonal-3 FeF$_3$ phase in Pattern 5[e] (S.G. $P4_2/mnm$)

R_p = 4.28%, R_{wp} = 5.70%

a = 4.7018(9) Å		c = 9.760(3) Å		V = 215.8(1) Å³		
Atom	Wyckoff symbol	x	y	z	B_{iso} / Å²	Occup.
Fe	2a	0	0	0	0.5	0.5013
Fe	4e	0	0	0.3209(9)	0.5	0.7493
F1	4f	0.231(2)	0.231(2)	0	0.5	1
F2	8j	0.332(1)	0.332(1)	0.2987(9)	0.5	1

Refinement results for the sodiated tetragonal-3 Na$_x$FeF$_3$ phase in Pattern 6[f] (S.G. $P4_2/mnm$)

R_p = 2.88%, R_{wp} = 4.03%

a = 4.720(1) Å		c = 9.866 (5) Å		V = 219.8(1) Å³		
Atom	Wyckoff symbol	x	y	z	B_{iso} / Å²	Occup.
Na	2a	0	0	0	0.5	0.4034
Fe	2a	0	0	0	0.5	0.4415
Fe	4e	0	0	0.336(2)	0.5	0.7793
F1	4f	0.227(3)	0.227(3)	0	0.5	1
F2	8j	0.294(2)	0.294(2)	0.373(1)	0.5	1

[a]The rutile FeF$_2$ ($P4_2/mnm$) is considered to be impurity phase. [b]The rutile FeF$_2$ ($P4_2/mnm$) and orthorhombic NaFeF$_3$ ($Pnma$) are considered to be impurity phases. [c]The rutile FeF$_2$ ($P4_2/mnm$) and trigonal FeF$_3$ ($R\bar{3}c$) are considered to be impurity phases. [d]The rutile FeF$_2$ ($P4_2/mnm$) and orthorhombic NaFeF$_3$ ($Pnma$) are considered to be impurity phases. [e]The cubic FeF$_3$ ($Pm\bar{3}m$) and rutile FeF$_2$ ($P4_2/mnm$) are considered to be impurity phases. [f]The orthorhombic NaFeF$_3$ ($Pnma$) and rutile FeF$_2$ ($P4_2/mnm$) are considered to be impurity phases.
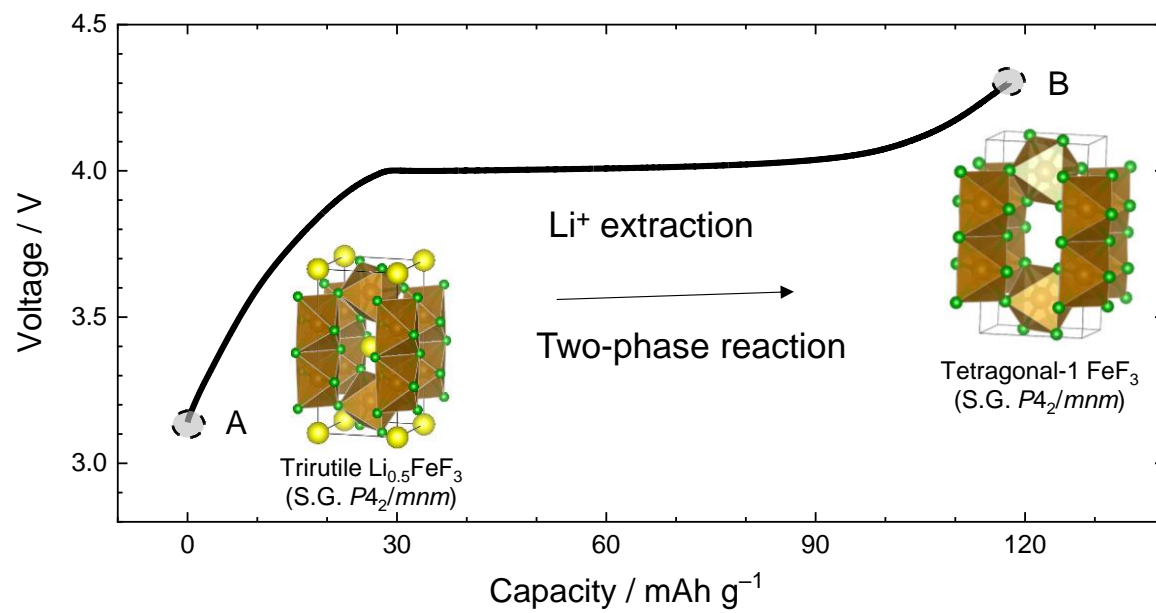
Figure 1. Schematic illustration for preparation of the tetragonal-1 FeF$_3$ electrode.
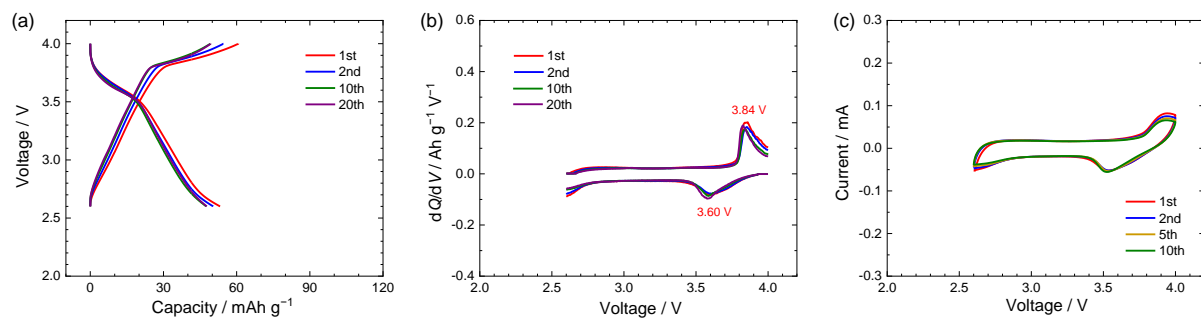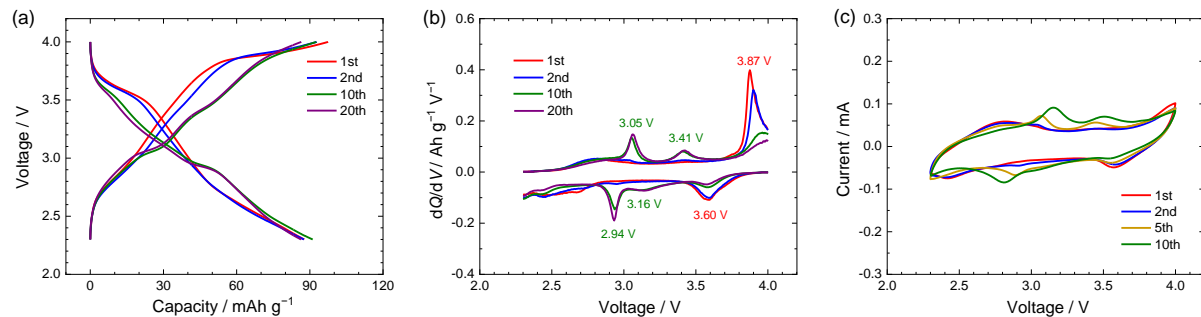
Figure 2. Charge-discharge properties of the Na/tetragonal-1 FeF$_3$ cell in the cut-off voltage of 2.6−4.0 V. (a) Charge-discharge curves at the rate of 21.4 mA g^{-1}. (b) The corresponding dQ/dV plots of the charge-discharge curves in (a). (c) CV at a scan rate of 0.1 mV s^{-1}. Electrolyte: Na[FSA]-[C$_2$C$_1$im][FSA] (30:70 in mol) IL. Temperature: 90 °C.

Figure 3. Charge-discharge properties of the Na/tetragonal-1 FeF_3 cell in the cut-off voltage of 2.3−4.0 V. (a) Charge-discharge curves at the rate of 21.4 mA g^{-1}. (b) The corresponding dQ/dV plots of the charge-discharge curves in (a). (c) CV at a scan rate of 0.1 mV s^{-1}. Electrolyte: Na[FSA]-[C_2C_1im][FSA] (30:70 in mol) IL. Temperature: 90 °C.
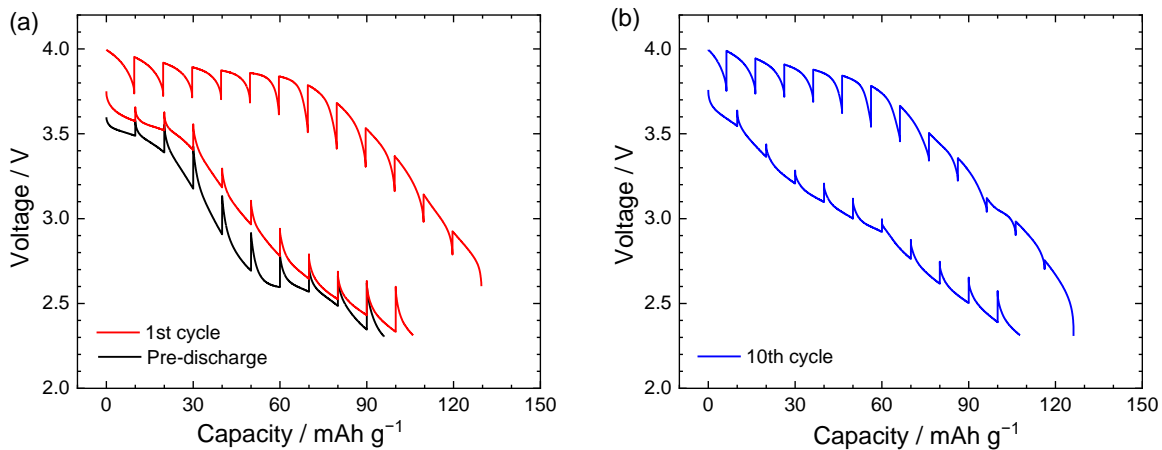
Figure 4. The GITT profile of the Na/tetragonal-1 FeF_3 cell in the cut-off voltage of 2.3−4.0 V. (a) Pre-discharge and 1st cycle. (b) 10th cycle after 9 cycles of galvanostatic charge-discharge at 21.4 mA g^{-1}. Electrolyte: Na[FSA]-[C_2C_1im][FSA] (30:70 in mol). Temperature: 90 °C.
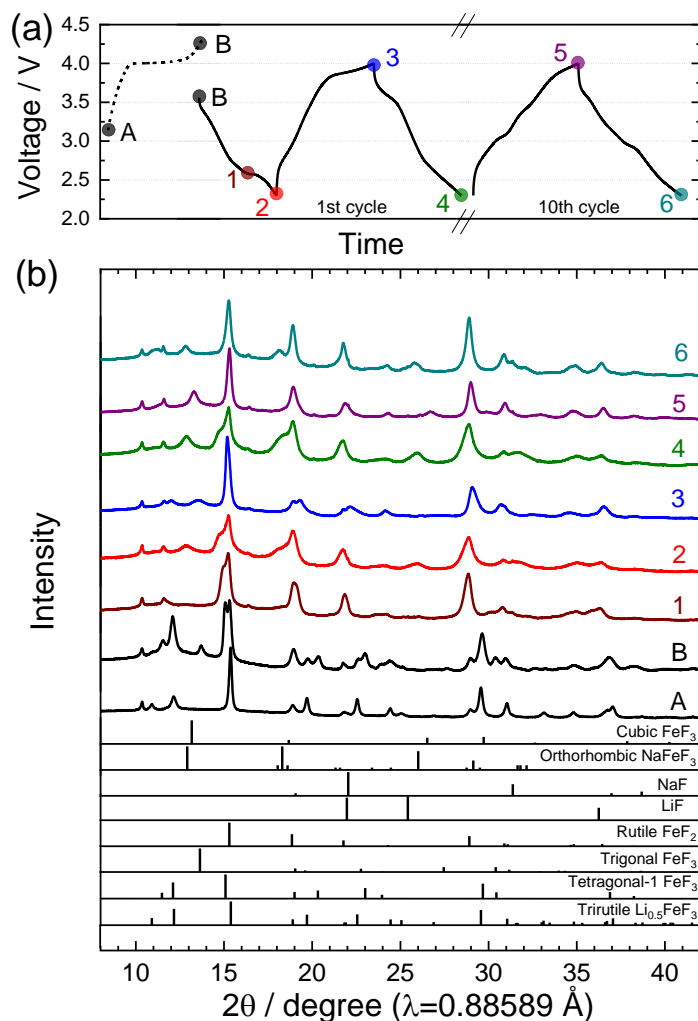
Figure 5. (a) A voltage-time profile of the XRD samples at different SOCs. (b) Synchrotron XRD patterns of the tetragonal-1 FeF_3 at different SOCs in comparison with the initial trirutile $Li_{0.5}FeF_3$. (1) Pre-discharged state at 2.6 V, (2) pre-discharged state at 2.3 V, (3) initial charged state at 4.0 V, (4) initial discharged state at 2.3 V, (5) 10th cycle charged state at 4.0 V and (6) 10th cycle discharged state at 2.3 V. Dashed line in (a) indicates the charge-discharge curve of the trirutile $Li_{0.5}FeF_3$ in the Li system. Solid line in (a) indicates the charge-discharge curve(s) of the tetragonal-1 FeF_3 in the Na system.
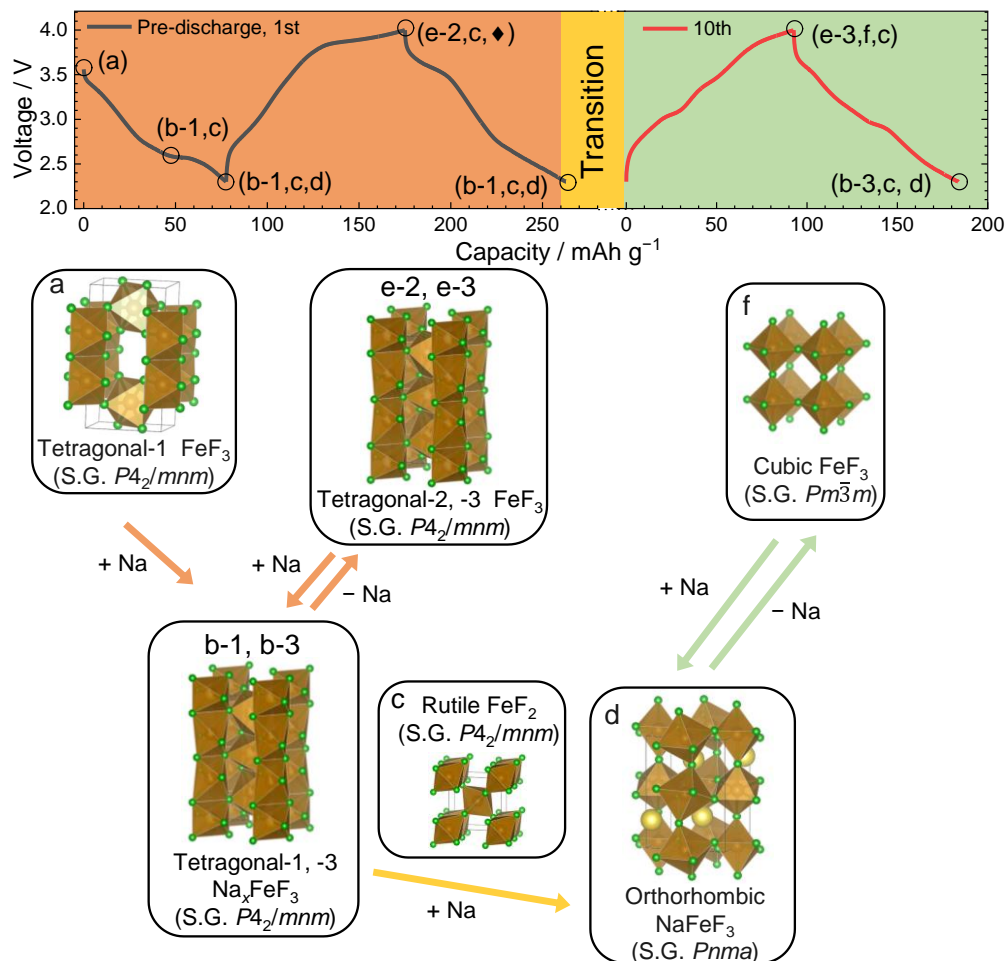
Figure 6. A schematic illustration of the reaction mechanisms of the tetragonal-1 FeF_3 during the sodiation-desodiation and the concomitant structural transition to the cubic FeF_3 phase. The b-1 and b-3 correspond to tetragonal-1 and -3 Na_xFeF_3 phases, respectively. The e-2 and e-3 correspond to tetragonal-2 and -3 FeF_3 phases, respectively. Desodiation from orthorhombic $NaFeF_3$ to tetragonal Na_xFeF_3 is limited, as orthorhombic $NaFeF_3$ tends to be desodiated into the cubic FeF_3. The formation of trigonal FeF_3, designated by ♦ in the figure, is a one-time occurrence.

ASSOCIATED CONTENT

Supporting Information. The Supporting Information is available free of charge on the ACS Publications website.

Electrochemical properties at room temperature using ionic liquid and organic electrolytes; pre-discharge curve; cycling performance; and fit to synchrotron XRD data (PDF).

AUTHOR INFORMATION

Corresponding Author

*E-mail: k-matsumoto@energy.kyoto-u.ac.jp

ORCID

Yayun Zheng: 0000-0003-1036-7650

Jinkwang Hwang: 0000-0003-4800-3158

Kazuhiko Matsumoto: 0000-0002-0770-9210

Rika Hagiwara: 0000-0002-7234-3980

Notes

Any additional relevant notes should be placed here.

REFERENCES

(1) Amatucci, G. G.; Pereira, N. Fluoride Based Electrode Materials for Advanced Energy Storage Devices. *J. Fluor. Chem.* **2007,** *128*, 243−262.

(2) Conte, D. E.; Pinna, N. A Review on the Application of Iron(III) Fluorides as Positive Electrodes for Secondary Cells. *Mater. Renew. Sustain. Energy* **2014,** *3*, 1−22.

(3) Omenya, F.; Zagarella, N. J.; Rana, J.; Zhang, H.; Siu, C.; Zhou, H.; Wen, B.; Chernova, N. A.; Piper, L. F. J.; Zhou, G.; Whittingham, M. S. Intrinsic Challenges to the Electrochemical Reversibility of the High Energy Density Copper(II) Fluoride Cathode Material. *ACS Appl. Energy Mater.* **2019,** *2*, 5243−5253.

(4) Nishijima, M.; Gocheva, I. D.; Okada, S.; Doi, T.; Yamaki, J.-i.; Nishida, T. Cathode Properties of Metal Trifluorides in Li and Na Secondary Batteries. *J. Power Sources* **2009,** *190*, 558–562.

(5) He, K.; Zhou, Y.; Gao, P.; Wang, L.; Pereira, N.; Amatucci, G. G.; Nam, K.-W.; Yang, X.-Q.; Zhu, Y.; Wang, F.; Su, D. Sodiation via Heterogeneous Disproportionation in FeF_2 Electrodes for Sodium-ion Batteries. *ACS Nano* **2014,** *8*, 7251–7259.

(6) Guntlin, C. P.; Zünd, T.; Kravchyk, K. V.; Wörle, M.; Bodnarchuk, M. I.; Kovalenko, M. V. Nanocrystalline FeF_3 and MF_2 (M = Fe, Co, and Mn) from Metal Trifluoroacetates and their Li(Na)-ion Storage Properties. *J. Mater. Chem. A* **2017,** *5*, 7383−7393.

(7) Xiao, A. W.; Lee, H. J.; Capone, I.; Robertson, A.; Wi, T. U.; Fawdon, J.; Wheeler, S.; Lee, H. W.; Grobert, N.; Pasta, M. Understanding the Conversion Mechanism and Performance of Monodisperse FeF_2 Nanocrystal Cathodes. *Nat. Mater.* **2020,** *19*, 644−654.

(8) Ni, D.; Fang, L.; Sun, W.; Shi, B.; Chen, X.; Li, H.; Wang, Z.; Sun, K. FeF$_2$@MHCS Cathodes with High Capacity and Fast Sodium Storage Based on Nanostructure Construction. *ACS Appl. Energy Mater.* **2020,** *3*, 10340−10348.

(9) Qian, J.; Wu, C.; Cao, Y.; Ma, Z.; Huang, Y.; Ai, X.; Yang, H. Prussian Blue Cathode Materials for Sodium-ion Batteries and Other Ion Batteries. *Adv. Energy Mater.* **2018,** *8*, 1702619

(10) Yuvaraj, S.; Oh, W.; Yoon, W.-S. Recent Progress on Sodium Vanadium Fluorophosphates for High Voltage Sodium-ion Battery Application. *J. Electrochem. Sci. Technol.* **2019,** *10*, 1−13.

(11) Liu, Z.; Xu, X.; Ji, S.; Zeng, L.; Zhang, D.; Liu, J. Recent Progress of P2-Type Layered Transition-Metal Oxide Cathodes for Sodium-ion Batteries. *Chemistry* **2020,** *26*, 7747−7766.

(12) Komaba, S.; Takei, C.; Nakayama, T.; Ogata, A.; Yabuuchi, N. Electrochemical Intercalation Activity of Layered NaCrO$_2$ vs. LiCrO$_2$. *Electrochem. commun.* **2010,** *12*, 355−358.

(13) Larcher, D.; Tarascon, J. M. Towards Greener and more Sustainable Batteries for Electrical Energy Storage. *Nat. Chem.* **2015,** *7*, 19−29.

(14) Grey, C. P.; Tarascon, J. M. Sustainability and In Situ Monitoring in Battery Development. *Nat. Mater.* **2016,** *16*, 45−56.

(15) Nayak, P. K.; Yang, L.; Brehm, W.; Adelhelm, P. From Lithium-ion to Sodium-ion Batteries: Advantages, Challenges, and Surprises. *Angew. Chem. Int. Ed. Engl.* **2018,** *57*, 102−120.

(16) Badway, F.; Pereira, N.; Cosandey, F.; Amatucci, G. G. Carbon-Metal Fluoride Nanocomposites Structure and Electrochemistry of FeF$_3$:C. *J. Electrochem. Soc.* **2003,** *150*, A1209−A1218.

(17) Doe, R. E.; Persson, K. A.; Meng, Y. S.; Ceder, G. First-Principles Investigation of the Li-Fe-F Phase Diagram and Equilibrium and Nonequilibrium Conversion Reactions of Iron Fluorides with Lithium. *Chem. Mater.* **2008,** *20*, 5274–5283.

(18) Yamakawa, N.; Jiang, M.; Key, B.; Grey, C. P. Identifying the Local Structures Formed during Lithiation of the Conversion Material, Iron Fluoride, in a Li Ion Battery: A Solid-State NMR, X-ray Diffraction, and Pair Distribution Function Analysis Study. *J. Am. Chem. Soc.* **2009,** *131*, 10525–10536.

(19) Yabuuchi, N.; Sugano, M.; Yamakawa, Y.; Nakai, I.; Sakamoto, K.; Muramatsu, H.; Komaba, S. Effect of Heat-Treatment Process on FeF_3 Nanocomposite Electrodes for Rechargeable Li Batteries. *J. Mater. Chem.* **2011,** *21*, 10035.

(20) Li, L.; Jacobs, R.; Gao, P.; Gan, L.; Wang, F.; Morgan, D.; Jin, S. Origins of Large Voltage Hysteresis in High-Energy-Density Metal Fluoride Lithium-ion Battery Conversion Electrodes. *J. Am. Chem. Soc.* **2016,** *138*, 2838–2848.

(21) Hua, X.; Eggeman, A. S.; Castillo-Martinez, E.; Robert, R.; Geddes, H. S.; Lu, Z.; Pickard, C. J.; Meng, W.; Wiaderek, K. M.; Pereira, N.; Amatucci, G. G.; Midgley, P. A.; Chapman, K. W.; Steiner, U.; Goodwin, A. L.; Grey, C. P. Revisiting Metal Fluorides as Lithium-ion Battery Cathodes. *Nature Mater.* **2021**, *20*, 841–850.

(22) Murugesan, V.; Cho, J. S.; Govind, N.; Andersen, A.; Olszta, M. J.; Han, K. S.; Li, G.; Lee, H.; Reed, D. M.; Sprenkle, V. L.; Cho, S.; Nune, S. K.; Choi, D. Lithium Insertion Mechanism in Iron Fluoride Nanoparticles Prepared by Catalytic Decomposition of Fluoropolymer. *ACS Appl. Energy Mater.* **2019,** *2*, 1832−1843.

(23) Ma, D.-l.; Wang, H.-g.; Li, Y.; Xu, D.; Yuan, S.; Huang, X.-l.; Zhang, X.-b.; Zhang, Y. In Situ Generated FeF_3 in Homogeneous Iron Matrix toward High-Performance Cathode Material for Sodium-ion Batteries. *Nano Energy* **2014,** *10*, 295–304.

(24) Zhang, R.; Wang, X.; Wang, X.; Liu, M.; Wei, S.; Wang, Y.; Hu, H. Iron Fluoride Packaged into 3D Order Mesoporous Carbons as High-Performance Sodium-ion Battery Cathode Material. *J. Electrochem. Soc.* **2018,** *165*, A89−A96.

(25) Yu, S.; Zhang, P.; Wu, S. Q.; Li, A. Y.; Zhu, Z. Z.; Yang, Y. Understanding the Structural and Electronic Properties of the Cathode Material $NaFeF_3$ in A Na-ion Battery. *J. Solid State Electrochem.* **2014,** *18*, 2071–2075.

(26) Kitajou, A.; Ishado, Y.; Yamashita, T.; Momida, H.; Oguchi, T.; Okada, S. Cathode Properties of Perovskite-type $NaMF_3$ (M= Fe, Mn, and Co) Prepared by Mechanical Ball Milling for Sodium-ion Battery. *Electrochim. Acta* **2017,** *245*, 424−429.

(27) Martin, A.; Doublet, M.-L.; Kemnitz, E.; Pinna, N. Reversible Sodium and Lithium Insertion in Iron Fluoride Perovskites. *Adv. Funct. Mater.* **2018,** *28*, 1−7.

(28) Martin, A.; Santiago, E. S.; Kemnitz, E.; Pinna, N. Reversible Insertion in $AFeF_3$ (A = K^+, NH_4^+) Cubic Iron Fluoride Perovskites. *ACS Appl. Mater. Interfaces* **2019,** *11*, 33132−33139.

(29) Zheng, Y.; Tawa, S.; Hwang, J.; Orikasa, Y.; Matsumoto, K.; Hagiwara, R. Phase Evolution of Trirutile $Li_{0.5}FeF_3$ for Lithium-ion Batteries. *Chem. Mater.* **2021,** *33*, 868−880.

(30) Toby, B. H. EXPGUI, A Graphical User Interface for GSAS. *J. Appl. Cryst.* **2001,** *34*, 210−213.

(31) Momma, K.; Izumi, F. VESTA 3 for Three-Dimensional Visualization of Crystal, Volumetric and Morphology Data. *J. Appl. Crystallogr.* **2011,** *44*, 1272−1276.

(32) Matsumoto, K.; Nishiwaki, E.; Hosokawa, T.; Tawa, S.; Nohira, T.; Hagiwara, R. Thermal, Physical, and Electrochemical Properties of Li[N(SO$_2$F)$_2$]-[1-Ethyl-3-methylimidazolium][N(SO$_2$F)$_2$] Ionic Liquid Electrolytes for Li Secondary Batteries Operated at Room and Intermediate Temperatures. *J. Phys. Chem. C* **2017,** *121*, 9209–9219.

(33) Matsumoto, K.; Hosokawa, T.; Nohira, T.; Hagiwara, R.; Fukunaga, A.; Numata, K.; Itani, E.; Sakai, S.; Nitta, K.; Inazawa, S. The Na[FSA]–[C$_2$C$_1$im][FSA] (C$_2$C$_1$im$^+$:1-ethyl-3-methylimidazolium and FSA$^-$:bis(fluorosulfonyl)amide) Ionic Liquid Electrolytes for Sodium Secondary Batteries. *J. Power Sources* **2014,** *265*, 36–39.

(34) Hwang, J.; Matsumoto, K.; Hagiwara, R. Na$_3$V$_2$(PO$_4$)$_3$/C Positive Electrodes with High Energy and Power Densities for Sodium Secondary Batteries with Ionic Liquid Electrolytes that Operate Across wide Temperature Ranges. *Adv. Sustainable Syst.* **2018,** *2*, 1−11.

(35) Matsumoto, K.; Hwang, J.; Kaushik, S.; Chen, C.-Y.; Hagiwara, R. Advances in Sodium Secondary Batteries utilizing Ionic Liquid Electrolytes. *Energy Environ. Sci.* **2019,** *12*, 3247–3287.

(36) Tawa, S.; Sato, Y.; Orikasa, Y.; Matsumoto, K.; Hagiwara, R. Lithium Fluoride/Iron Difluoride Composite Prepared by a Fluorolytic Sol–Gel Method: Its Electrochemical Behavior and Charge–Discharge Mechanism as a Cathode Material for Lithium Secondary Batteries. *J. Power Sources* **2019,** *412*, 180–188.

(37) Yamada, Y.; Doi, T.; Tanaka, I.; Okada, S.; Yamaki, J.-i. Liquid-Phase Synthesis of highly Dispersed $NaFeF_3$ Particles and their Electrochemical Properties for Sodium-ion Batteries. *J. Power Sources* **2011,** *196*, 4837–4841.

(38) Kitajou, A.; Komatsu, H.; Chihara, K.; Gocheva, I. D.; Okada, S.; Yamaki, J.-i. Novel Synthesis and Electrochemical Properties of Perovskite-type $NaFeF_3$ for a Sodium-ion Battery. *J. Power Sources* **2012,** *198*, 389–392.

(39) Dimov, N.; Nishimura, A.; Chihara, K.; Kitajou, A.; Gocheva, I. D.; Okada, S. Transition Metal $NaMF_3$ Compounds as Model Systems for Studying the Feasibility of Ternary Li-M-F and Na-M-F Single Phases as Cathodes for Lithium–Ion and Sodium–Ion Batteries. *Electrochim. Acta* **2013,** *110*, 214−220.

(40) Li, C.; Yin, C.; Mu, X.; Maier, J. Top-Down Synthesis of Open Framework Fluoride for Lithium and Sodium Batteries. *Chem. Mater.* **2013,** *25*, 962–969.

TOC graphic